Natural ageing in Al-Mg-Si alloys –
a process of unexpected complexity

John Banhart[1,2], Cynthia Sin Ting Chang[1], Zeqin Liang[1], Nelia Wanderka[1],
Matthew D.H. Lay[3], Anita J. Hill[3]

[1]Helmholtz Centre Berlin for Materials and Energy, Hahn-Meitner-Platz 1, 14109 Berlin, Germany

[2]Technische Universität Berlin, Materials Science and Technology, Hardenbergstr. 36, 10623 Berlin, Germany

[3]CSIRO Materials Science and Engineering, Clayton, Victoria, Australia

The natural ageing behaviour of pure ternary Al-Mg-Si alloys is investigated by measuring hardness, electrical resistivity and positron lifetime, as well as carrying out thermal analysis and atom probe microscopy. It is found that several distinct temporal stages of natural ageing can be distinguished in which one of these quantities shows a characteristic behaviour and that these times coincide for many of these measurements. The rate of change in the measured data is correlated with proposed solute dynamics during natural ageing for both ageing that takes place prior to artificial ageing (natural pre-ageing) and post artificial underageing (natural secondary ageing) heat treatments. Controlling factors for solute dynamics are discussed.

Author information

Prof. Dr. John Banhart, Head of Institute

Dr. Cynthia Sin Ting Chang, Scientist

Zeqin Liang, PhD Student

Dr. Nelia Wanderka, Senior Scientist

Dr. Matthew D.H. Lay, Postdoctoral Fellow

Dr. Anita J. Hill, Chief Research Scientist

Text and Graphic for Table of Contents

Pure Al-Mg-Si alloys are naturally aged after solutionising and quenching. Measurements of hardness, electrical resistivity, positron lifetime, thermoanalysis and atom probe tomography suggest at least four different stages of solute and vacancy clustering and early precipitation. The observed correlations between natural pre-ageing, artificial ageing and secondary ageing allow for the discussion of solute dynamics in these alloys.
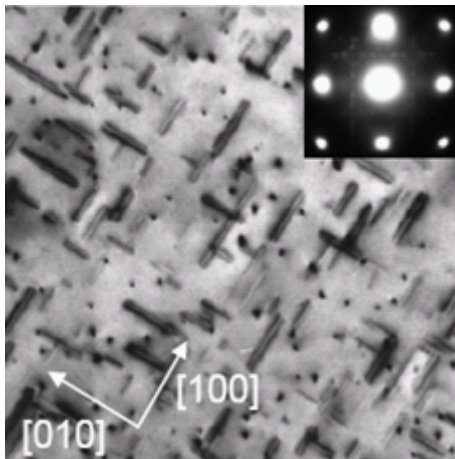
BF-TEM image of alloy F (AA for 540 min after 10,000 min pre-ageing)

1 Background

Alfred Wilm paved the way for the use of aluminium alloys as engineering material more than 100 years ago when he accidentally discovered ageing in an Al-Cu-Mg alloy, which belongs to what is known today as the '2000 series' of aluminium-based engineering alloys.[1] It took about 30 years to explain how age hardening works. Many researchers contributed, but only in 1938 Guinier and Preston could prove that small precipitates that were invisible in the microscopes available in those days were responsible for hardening.[2] Al-Mg-Si alloys had already been developed in the 1920s.[3] They can be hardened by '*artificial*' ageing – i.e by baking the solid solution at 150°C to 180°C after quenching. Such '6000 series' alloys are now widely used versatile materials due to their potential to be aged to medium strength while having good metal forming properties in the non-aged state. In addition, corrosion and welding properties are reasonable, costs are moderate and handling is simple. They have found many applications in the transport industry (automotive, railway), architecture and consumer goods industry.

One of the peculiarities of Al-Mg-Si alloys, the adverse effect of room temperature '*natural*' ageing on a subsequent artificial ageing step, was discovered a long time ago. In the year 1939, one year after Guinier and Preston had published their explanation of age hardening in Al alloys, Brenner and Kostron described this effect in an alloy containing 0.8 wt.% of both Mg and Si and write: "*Trotzdem die Entdeckung der ersten vergütbaren Aluminiumlegierungen nun schon Jahrzehnte zurückliegt, ist unsere Kenntnis über den Mechanismus, auf dem die Vergütbarkeit beruht noch recht lückenhaft*" (*Although the discovery of the first age hardenable aluminium alloys already lies back a few decades, our knowledge about the mechanism of age hardening is still rather fragmentary*).[4] This statement is in parts still valid today although, of course, we know a lot more about these alloys than 70 years ago.

The precipitation sequence in Al-Mg-Si alloys has been investigated by many researchers and includes the stages listed in Figure 1. Such sequences are frequently given in publications or books,[5] but one should remember that this is not a particular sequence valid for any temperature. Some of the phases might not occur at all at too low a temperature or may evolve into others almost instantaneously at too high a temperature and there may be ranges of co-existence of more than one phase. The exact precipitation sequence depends on the alloy composition (excess in Mg or Si, or balanced alloy[6]) and the possible presence of

additional elements (Cu, Mn, Fe, …). This number of caveats helps explain the confusing situation encountered in the literature, characterised by different designations, different mixtures of phases found, etc.

In the literature, work on 6000 alloys can be divided into two main topics:

1. 'High temperature' work on the evolution of structures during artificial ageing at 150°C or higher. Such work focuses on:

   - Structural characterisation of hardening particles,[6,7,16,17,40]
   - Study of precipitation sequence and transformation pathway,[6,7,55,58]
   - Influence of alloy composition,[56]
   - Interrelationship between hardening particles and mechanical properties,
   - Influence of thermal and mechanical history on hardening, i.e. influence of storage at lower temperatures (often 'negative' or deleterious) or influence of deformation (mostly 'positive' or beneficial) on the hardening potential of the alloy.[49,57]

2. 'Low temperature' work on the processes directly after quenching at 'room temperature', i.e. temperatures well below the range of artificial hardening, typically below 100°C. This includes:

   - Studies of vacancy migration and atomic clustering processes,[11,22,33,62]
   - Structure and composition of clusters,[14,16,46]
   - Effect on subsequent artificial ageing – e.g. the already mentioned negative effect.[49]

In order to clarify the formation of hardening precipitates, a number of imaging methods have been applied successfully, namely

   - Transmission electron microscopy (TEM) for identifying larger precipitates and measuring their density,
   - High-resolution (HR) TEM for revealing their structures,
   - 3D atom probe (3DAP) for measuring chemical compositions including the Al content in precipitates.

What has become evident from studies of the past 10 to 15 years is the central role of Si precipitation for the development of the nanostructure. It was observed that already in early

stages of ageing the silicon atoms form a network around which the precipitate evolves.[8] Diffusion processes change the concentration of both Al and Mg as the precipitate evolves. Researchers claim to have discovered that Si arranges into double pillar structures that remain invariant during further growth,[9] but there is a dispute whether this is a universal feature in a broader group of alloys.[51]

Natural ageing (NA) is technologically not relevant for 6000 series alloys because these alloys are always artificially aged (AA). However, because the NA that occurs during processing can have a 'negative' effect on AA, it is worthy of detailed study. Of all the imaging techniques, only 3D atom probe has the potential to resolve the clusters formed during natural ageing. Indirect techniques such as thermal analysis, resistivity measurement, X-ray scattering, and positron annihilation spectroscopy can be utilised to build a comprehensive picture of phase evolution. Experience shows that one such indirect technique is not powerful enough to clearly reveal the subtle changes in a quenched alloy during 'room temperature' ageing and that many of these methods have to be applied. Extracting and comparing information from the literature, however, is difficult due to the use of too many different alloys and ageing conditions. This complexity is why an effort has been started to do such analyses on a few pure ternary alloys while keeping the variety of heat treatments to a minimum.

2   Available methods and the "6000 alloy problem"

2.1   General problem

The study of 6000 series alloys is complicated by two facts. Firstly, the content of Mg and Si is always very low, i.e. ≤ 1.5 or ≤ 1.2 wt.% for each of the elements Si and Mg, respectively. This implies that any element-sensitive probe will yield a *low signal-to-noise ratio* (SNR). Secondly, Mg, Al and Si are neighbouring elements in the periodic table. The interaction of X-rays and electrons usually scales with some power of the electron density which is then very similar for the three elements considered. Therefore, element *contrast is low* in electron microscopy as far a Z-contrast is concerned and X-rays are diffracted from the different atoms in a similar way. X-ray small-angle scattering that is a very useful technique to discover nm-sized fluctuations in electron density yields weak signals from clusters enriched in Mg and Si that are embedded in an Al-rich solid solution because scattering is governed by the scattering length density difference between the cluster and the matrix which

is very small.[38] Attempts to utilise anomalous scattering at the absorption edges of an individual element run into difficulties because a) the absorption edges are at very low energies, see Table 1, implying that very thin samples (a few µm) and windowless beamlines would have to be used, and b) the absorption edges are very close to each other, implying that fluorescence radiation would create a big background whenever the energy is above the K edge of Al which is the case when tuning to the K-edge of Si. Unfortunately, small-angle neutron scattering has to deal with a similar problem since the scattering lengths of the three elements are also quite similar, see Table, 1 and there are no isotopes with a largely different scattering length that could be used to enhance contrast. Altogether, this is the reason why age hardening in Al-Cu has been studied more often and more successfully in the past although the technological and economical importance of the Al-Mg-Si alloy family exceeds that of Al-Cu alloys.

2.2 Available experimental methods

2.2.1 Direct imaging methods

Obtaining direct images from precipitates is the most convincing proof for their existence and if one can obtain some properties from images the benefit can be very large. Two methods have been applied to some extent to image precipitates in 6000 alloys, namely *transmission electron microscopy (TEM)* and *3D atom probe (3DAP)*.

It is believed that precipitates formed during natural ageing cannot be made visible by TEM. Bright-field HRTEM images of an Al-Mg0.65Si0.7 alloy naturally aged for 70 days show hardly any features and the authors report that the same applied to another alloy and that the diffraction pattern also did not show any trace of a precipitate.[16]

3DAP can provide information about precipitates on two levels either by imaging the precipitated objects directly after applying an appropriate cluster identification procedure to the AP data set, or, in case this does not yield a reliable result, on the level of a statistical analysis providing correlations between the atoms only via so-called contingency tables. 3DAP has been used to investigate naturally aged Al-Mg-Si alloys by various groups. The Al-Mg0.65Si0.7 sample naturally aged for 70 days exhibits no visible clusters, but the contingency table analysis clearly shows the correlation between Mg and Si atoms.[16] In contrast, Serizawa et al. report that clusters formed in AlMg0.95Si0.81 alloys after natural

ageing between 4 weeks and 2.5 years can be identified and even analysed with respect to cluster size, composition and interatomic bonding conditions.[14,46,60]

2.2.2 Methods probing local environments

There are a number of methods that allow us to derive information about the local neighbourhood of a given species of atoms in a sample but without providing any spatial resolution. One of these methods is *nuclear magnetic resonance* spectroscopy (NMR) that has been successfully used to study precipitation effects, e.g. in Al-Cu alloys, by detecting the changes in the minority atom (Cu) NMR signal caused by varying local environments.[18] Unfortunately, in Al-Mg-Si alloys neither Mg nor Si provide enough sensitivity to yield a useful signal.

X-ray absorption fine structure (XAFS) is another such probe that is being applied, e.g. to Al-Cu alloys.[19] In Al-Mg-Si alloys, however, only the Mg absorption edge would yield useful information but this edge is difficult to utilize due to the low K-edge energy, see above.

A third method that is sensitive to local environments is *positron annihilation spectroscopy* (PAS). Both positron lifetime spectroscopy (PALS) and Doppler broadening (DB) spectroscopy have been used to study precipitation phenomena in Al-alloys.[20] Natural ageing in Al-Mg-Si has been studied by few authors only,[11,21-23] but up to now the results do not allow for many conclusions about the mechanism of natural ageing. Positron lifetimes reflect the electron densities around the annihilation sites of positrons in a material and allow, in principle, the derivation of vacancy densities and the atomic configuration around vacancies and other positron trapping sites. The strength of the method is its reproducibility and sensitivity, its weakness is that positrons can annihilate at different sites and it is very difficult to separate a mixture of different lifetimes. Moreover, the lifetime one expects from different sites is experimentally only known for the bulk material and monovacancies and for vacancy clusters via theoretical calculations,[48] whereas the lifetimes in other traps (e.g. vacancy solute complexes) are not known very well and await the guidance provided by rigorous calculations.

Small-angle X-ray scattering (SAXS) has been used to study artificial ageing in 6000 alloys but the method suffered from a poor SNR in this case.[34] S*mall-angle neutron scattering* (SANS) has also been applied and yielded a stronger signal,[31,32] but no application to natural ageing is known. The quantitative analysis of small-angle scattering data always

relies on additional information such as particle shapes and compositions which are not available for early stages of precipitation in Al-Mg-Si alloys. Together with the weak scattering signal, see above, this will imply that only qualitative conclusions can be expected.

2.2.3 Methods providing globally averaged properties

Differential thermal analysis has been used by many groups to elucidate the cluster formation process during natural ageing of 6000 alloys.[14,22,27,33,63] After quenching, samples are naturally pre-aged for different times before they are heated up at a constant heating rate while measuring the heat released or absorbed. The difference between the measurement on samples with and without pre-ageing provides a measure for the precipitation process during natural ageing. DSC measures an average over the entire sample.

The same applies to the *electrical resistivity* which is extremely sensitive to very small changes of the atom configuration induced by atomic diffusion and has been used to characterise ageing in Al-Mg-Si alloys.[10,11,26,61] Unfortunately, the signal obtained is not easy to relate it to microscopic features.

Mechanical properties, e.g. *hardness* or *tensile strength,* that can be easily measured in various stages of natural ageing also reflect the resistance to dislocation movement built up by clusters and emerging precipitates, but again, nanoscale features cannot be directly derived.

3   Sample preparation

Two alloys of the Al-Mg-Si system were studied: one with a low content in both Si and Mg (denoted H), one with a higher one (denoted F). Past research has shown that H does not show the negative effect and that F shows the negative effect.[49] The H material resembles commercial 6060 alloys without any other elements except for Al, Mg and Si, the F material composition comes close to alloys such as 6111 or 6082. The alloys were prepared by Hydro Aluminium (Bonn) from very pure elements. The final product came as a rolled sheet of 1 mm thickness and was chemically analysed by sparc optical emission spectroscopy (OEM) after manufacture. The compositions of both alloys are given in Table 2.

Solution heat treatment was carried out at 535-540°C for typically 30 min or 60 min in air, after which the samples were quenched into ice water. For studies of natural ageing, the samples were further processed very fast so that the first hardness, resistivity or positron lifetime data could be obtained with as little delay as possible, typically <2 min (see results

section). For the electrical resistivity measurement the sheets were drawn to wires of 0.8 mm thickness.

4 Experimental studies using different techniques

Throughout this chapter we will use the term *natural ageing* (NA) for any ageing at 'room temperature' which ranged from 18°C to 21°C in the experiments presented. *Artificial ageing* (AA) was carried out at 180°C. If NA was performed before AA, we use the expression *natural pre-ageing* (NPA), if it was carried out after AA, the term *natural secondary agein*g (NSA) is used.

4.1 Natural ageing (NA)

We first present studies of simple NA at constant 'room temperature' directly after quenching. NA in combination with AA will be presented in 4.2.

4.1.1 Hardness

The hardness evolution during NA was investigated for the two alloys H and F. Figure 2 shows that the hardness for alloy F initially increases much faster than that of alloy H. Moreover, different stages can be distinguished for alloy F. The density of the data points does not allow to clearly identify whether there are 2 or 3 different stages. One interpretation (marked '1' Figure 2) involves a stage of fast initial hardening up to 85 (+30,−20) min, after which the hardening process slows down and the further hardening course becomes approximately parallel to the course of alloy H. Hardness as a function of log(t) shows approximately linear slopes for both alloys. Note that for t→0 the flat dotted line indicates that the hardness starts from the finite value corresponding to the solid solution. For both the alloys and at any time the hardness vs. time is nonlinear despite the impression created by the logarithmic time scale. The other interpretation (marked '2' in Figure 2) implies an intermediate hardening range from 50±10 min to about 800±200 min after quenching for alloy F.

The data shown for t > 60 min is compatible with that given in the literature,[10] where, however, the change from rapid hardening to slow hardening rate cannot be seen since the measurements start after 60 min. In some studies a change in slope is observed too, but after a much longer time of NA.[15,41,42,44] The latter reference,[42] however, gives one example of an earlier change in an alloy rich in Si, thus demonstrating the large variability of hardening

kinetics. Some studies, mostly on engineering alloys containing other elements than Mg and Si, do not show a clear change of hardening rate at all.[4,43] The very fast ageing rate in our alloy F can be explained by the purity of the metals used, since some additional elements are known to slow down natural ageing due to trapping of vacancies after quenching which are then no longer available to mediate the early clustering process.[45]

The increase in hardness during natural ageing is caused by the growth of a high density of clusters that have a higher shearing resistance to dislocations than the supersaturated matrix. The early fast process gradually changes to the later stage slow process over the interim period (50 – 800 min) which appears to be a combination of the fast and slow processes. The change in hardening rate from fast to slow can be explained both by a decrease in the growth rate and in the shear resistance of the clusters, the latter caused by a change in composition.

Natural ageing in Al-Mg-Si alloys has been discussed such that it is initially silicon that dominates cluster formation due to its higher diffusivity and lower solubility in aluminium and that in a later stage magnesium starts contributing to cluster formation.[33]Although this picture is directly supported only by data about chemical changes within precipitates formed at higher temperatures, it is commonly assumed to be valid at room temperature too. Accepting this assumption, initial clustering would lead to Si-rich clusters which increase hardness at a fast rate. Later, i.e. after ~50 minutes, some fraction of these would begin to enrich in Mg and cause further hardening (50 min – 800 min), but at a lower rate, until finally all clusters are enriched with Mg and further cluster growth is dominated by Mg diffusion (the slow rate process for times >800 min). Also worthy of note is the similarity of the rate of hardness increase in the late stage of Alloy F with that over the measured lifetime of alloy H. This slow process has been tentatively attributed, in alloy F, to the diffusion of Mg to Si-Mg co-clusters. The lack of a fast process in alloy H is likely due to the much lower percentage of Si in alloy H (50% less than in alloy F). It is possible that rather than Si clustering preceeding Si-Mg co clustering, the composition of alloy H which is lean on Si results in Si finding Mg with equal or greater probability than Si finding Si. This probability of clustering and pathway of clustering and co-clustering are the subject of current modelling studies. However, direct proof for this picture is lacking at this point of the discussion.

4.1.2 Electrical resistivity

The electrical resistivity of a thin drawn wire (diameter 0.8 mm) of alloy F was measured *in-situ* as a function of NA time (21°C) after quenching of the wire into ice water and placing it in a water-filled dewar. A four-point measurement was applied and a value was obtained every 0.3 s. Figure 3 shows that the resistivity increases at any instant and that again distinct stages can be distinguished by their slopes that appear linear if the time is used on a logarithmic scale. We observe an initially fast increase of resistivity. After about 85±15 min, the slope changes to a lower value within roughly 30 min and the resistivity continues to increase up to the end of the period investigated. Possibly, another change in slope after about 1000±300 min can be detected. The long-term data in Figure 3 is a separate set, and this imposes restrictions on a precise determination of the time the second slope changes into the third. Individual data points for alloy H are also given. Obviously the resistivity change is much smaller than in alloy F.

These findings are in agreement both with in-situ measurements reported in the literature[15] and with recent measurements,[11] where very similar alloys were investigated ex-situ, i.e. the measurements were carried out at 77 K temperature and the sample was allowed to anneal at room temperature between two measurements. A change of slope is clearly observed after 60 min and 110 min in two measurements which is in agreement with our result. Other researchers have found very similar results,[15,26] others find that the change from the fast to the slow increase takes place later in a similar alloy containing impurities.[50,52] Seyedrezai et al. claim that they can identify a further early logarithmic stage when they measure at 0°C[11] and propose a model for the logarithmic behaviour in general.[29] Figure 3 seems to suggest that such an early stage exists here too, but to our judgement it is difficult to decide whether the resistivity in this range is proportional to log(t) or rather a linear function (that appears exponential in this representation). If a cross-over between two stages existed, it could be at any time between 7 min and 12 min after quenching.

Most reactions in non-equilibrium alloys reduce resistivity, such as the formation of long range order, formation of most metastable and stable phases and the corresponding solute depletion of the matrix and annealing out of vacancies.[35,39] Here, the resistivity does not decrease at any point, indicating that clusters are formed in a size range where incoherent electron scattering is enhanced because the mean free path of the electrons is in the range of the cluster size.[64] As for hardness, there is an initial fast reaction that changes into a slower

one after 85 min which is very similar to the time the hardness course changes its slope. It is reasonable to assume that the same change of the rate of cluster growth or cluster composition postulated as a reason for the change of hardness, influences resistivity as well. More specifically, it is assumed that in the regime of fast increase the diffusion of solute atoms is easy since enough vacancies are available for solute transport. Although vacancies do form vacancy/solute complexes, such pairs could break up and allow diffusion of other solute atoms, especially silicon. In the later stage, the vacancies are postulated to become increasingly trapped in larger solute/vacancy complexes also containing magnesium, and diffusion slows down.[26] In summary, alloy F shows similar stages in hardness and resistivity that relate to cluster formation and growth and solute diffusion. The fast process (at shorter times up to ~50 or 85 minutes) is attributed to Si diffusion dominated cluster formation and growth and the slower process is attributed to Mg diffusion dominated co-cluster growth.

4.1.3 Differential thermo-analysis (DSC)

DSC was carried out on samples of alloy F using a Netzsch 404C differential scanning calorimeter. The DSC study confirmed earlier findings of other researchers published in the literature.[27] Figure 4(a) shows three DSC traces, one for an alloy F specimen inserted into the DSC apparatus within 1 min after quenching and measuring with 10 K/min heating rate, as well as another two samples which were left to age at room temperature for 60 min and 10,000 min (1 week). Note that these peaks are exothermic such that they are indicative of phases able to form once the thermal energy supplied during the DSC scan enables a phase transformation (endothermic peaks observed from ~180 – 240°C (not shown) are the dissolution of phases). For the as-quenched sample a decomposition of the DSC curve into three Gaussians is shown. Obviously, formation of clusters in this sample occurs at two temperatures, a first, lower temperature reaction at approximately 50°C and a second higher temperature reaction at approximately 80°C. If time at 'room temperature' (natural ageing) allows the full development of clusters and co-clusters then the exotherms will disappear, as no more formation will occur on heating in the DSC. The formation of the initial clusters is clearly mostly complete after 60 min as this endothermic peak at 50°C is no longer significantly present. It is also clear from Fig 4a that the clusters formed at higher temperature need more thermal energy to form if the precursor (lower temperature) clusters are already fully formed. The second exothermic peak moves to higher temperature and reduces in magnitude with natural ageing time up to 10,000 min. Others have observed these features in

DSC studies of 6000 series alloys and have attributed the ~50°C reaction to mainly Si clustering and the ~80 – 120°C reaction to clustering reactions in which Mg is added.[33]

Figure 4(b) summarises some of the findings on alloy F and also results on other Al-Mg-Si alloys taken from the literature. Obviously, even though the alloy compositions differ, the basic phenomena are the same: we find an initial clustering reaction which has completed after about 60 min and a second one that has almost come to an end after 10,000 min (1 week). While for the first reaction the peak temperature is constant, it increases for the second. The fact that after 60 min the first reaction has completed, makes the interpretation plausible that the stage of rapid hardness and resistivity increase is associated with that reaction and that during the second reaction the slower processes occur.

4.1.4 Positron annihilation lifetime spectroscopy (PALS)

The average positron lifetime was measured in samples at 'room temperature' (18°C) as a function of time directly after quenching into ice water. The experiments will be presented in detail elsewhere.[12] In Figure 5, the principle course of average positron lifetime found in Al-Mg-Si alloys is shown. We observe up to four distinct stages: in alloy F (but not in H) a short period (7 min to 10 min) of constant (or even very slightly increasing) lifetime between 0.222 and 0.227 ns, then a period of lifetime decrease (≈60 min for alloy F, ≈80 min for alloy H) down to 0.213 ns, after which the lifetime increases again for typically 800 – 1000 min up to 0.217 ns. This increase then reverses into another decrease which continues for longer than 10,000 min and seems to approach the lifetime measured in as-received equilibrium-state alloys which is 0.212 to 0.213 ns. The scatter of results between individual samples of the same alloy composition is large for the period immediately after quenching (but the trend is similar). The scatter becomes lower in later stages, indicating that effects during quenching, that are hard to keep constant, do influence lifetime.

The interpretation of this very unusual behaviour (the only time a non-monotonic behaviour of lifetime during natural ageing has been reported is for Al-Zn-Mg[36]) is not straight-forward and in parts still speculative and will be provided in a separate publication.[12]

Immediately after quenching there is a large density, i.e. atomic fraction 10^{-5} to 10^{-4}, of free non-equilibrium vacancies in the alloy. Unlike pure metals where these vacancies gradually annihilate at grain boundaries, dislocation loops or the sample surface, in alloys, containing typically 10^{-2} solute atoms such as Mg and Si, vacancy solute complexes are

formed very quickly, long before we can measure the first positron lifetime (which is approximately 2min to 3 min following quench). The initial lifetimes measured (0.220 to 0.230 ns depending on the alloy) therefore express the lifetime of such complexes and not that of free vacancies in Al that would give rise to lifetimes of around 0.250 ns or more. The stage of lifetime decrease in a period up to ~60-80 min coincides with characteristic times found using DSC, resistivity and hardness measurement. Accepting the assumption that silicon clustering occurs first, these clusters could be responsible for the initial decrease in positron lifetimes by 0.010 to 0.020 ns, depending on the alloy, see discussion in 4.2.2. The ensuing lifetime increase after 60-80 min could then correspond to the addition of Mg to existing Si-clusters (co-clustering) or the formation of new Mg-rich clusters. The origin of the final decrease starting about 800 minutes after quenching is not clear. Perhaps ordering phenomena within the clusters formed begins to occur. These results could imply that vacancies that were previously trapped in the clusters are finally released and diffuse to sinks. This interpretation still remains speculative without any additional evidence from other methods.

4.1.5 Small-angle neutron scattering (SANS)

Small-angle neutron scattering is sensitive to fluctuations in a heterogeneous matrix that range from 2 to 300 nm in size. A prerequisite for scattering is a large difference in scattering length density between the matrix and the inclusions which, e.g., can be clusters enriched in Mg and/or Si. Provided that the scattering length density is known, a quantitative analysis of the particle size distribution can be carried out based on a model for the shape of the inclusions,[25] If, however, the little is known about the inclusions, only their typical size can be estimated from the scattering curve I(Q), using the relation R = $2\pi/Q$ as indicated in Figure 6.

We carried out SANS experiments on alloy F samples directly after quenching and after different storage times at room temperature. The SANS beamline V4 of the Hahn-Meitner Reactor (Berlin) was used. The sample thickness was 7 mm. The measurements were carried out at room temperature and took about 240 min each so that the 'as-quenched' sample is measured as an ensemble over the first 240 min from quench and includes at least two stages of development (clustering and some co-clustering) according to the results of other techniques presented above. One can clearly see a difference between the scattering curves obtained after an average over 240 min and after approximately 86,000 min. This difference must be attributed to growing local compositional change ('clustering') that occurs

during ageing, ranging between 2 and 6 nm in size. However, the difference is small and located in the regime of very small count rates close to the instrumental background. Additional measurements based on shorter natural ageing times gave less clear results. Thus, it can be concluded that SANS is not the appropriate technique to resolve clustering phenomena in early stages.

4.1.6 Atom probe (3DAP)

3D atom probe can resolve individual atoms and identify their type and has therefore played an important role in identifying clusters that are formed in early stages of ageing and to measuring their composition.

We studied natural ageing of alloy H and F using 3DAP. The experimental details can be found in the literature where one result related to alloy H has been discussed.[13] Here, we studied two alloys F that were naturally aged after quenching for 10,000 min (1 week) and 260,000 min (6 months). The direct reconstruction of the Mg and Si atom position appears random and application of a cluster search algorithm does not reveal clusters, see Figure 7. The contingency table analysis based on blocks of 50 atoms, however, demonstrated the same type of correlation as reported in the literature,[16] namely the observation that finding one (or two) Mg(Si) atoms in a given block implies a higher probability to find also one(or two) Si(Mg) atoms, respectively. Thus, after prolonged natural ageing, clusters containing both Mg and Si have formed. The same situation was observed after 10,000 min of natural ageing. Because contingency analysis does not provide any information about the size and composition of possible clusters, this information is not sufficient on its own but can support the interpretation of results obtained by other methods.

4.2 Artificial ageing after natural ageing

We now discuss some of the phenomena occurring during natural ageing by studying their impact on a subsequent artificial ageing step.

4.2.1 Hardness

Figure 8 gives the hardness evolution of alloy F during artificial ageing at 180°C. The different curves represent different natural pre-ageing (NPA) times at 'room temperature' after quenching. The main observation is that NPA has an adverse effect on hardness evolution during AA, the so-called 'negative' effect reported many times in the literature.[4]

We observe that both the rate of initial hardening is reduced and the final peak hardness drops from 120 to 110 HV.

What is new here is that the negative effect is observed already for very short NPA times. Even after 2 min the initial slope starts to reduce, for 5 min, 7.5 min and 10 min the effect gets stronger and for 18 min of NPA the hardening course is very close to the course observed for 10,000 min of NPA. In the literature [4,10,49], the negative effect of NPA sets in much slower, probably due to the additional elements contained in the engineering alloys used there that bind vacancies and slow down NA.

Just to obtain a quantitative measure for the loss in hardening response, we read the values for 60 min of AA and plot them as function of NPA time in Figure 8(b). Moreover, we determine the time needed to reach 90HV hardness value. Both measures for the loss of AA hardenability express the same behaviour. Moreover, the observed changes in the positron lifetime change during secondary ageing – discussed in the next section – corresponds well with the loss in hardness response. This provides a hint that there is a common reason for these findings.

4.2.2 Transmission electron microscopy

Figure 9 shows bright-field transmission electron microscopy images of alloy F aged for 540 min after solutionising and quenching. The difference between (a) and (b) is that in (b) the alloy was stored at 'room temperature' before AA for 10000 min ($\approx$1 week). In both cases, the needle-shaped precipitates – most likely β'' – in three different orientations can be seen. Visual inspection of the images reveals that the latter alloys exhibit a coarser precipitate structure. A more detailed quantitative analysis involves measuring the length and density of precipitates, see Table 3. Clearly, NPA at 'room temperature' prior to AA leads to a lower density but higher volume fraction of longer and thicker precipitates that are less effective in hindering dislocation movement. This is a direct manifestation of the 'negative effect' as reported in the literature before.[54] The main change is observed between 5 and 18 min of NPA which is in line with the results displayed in Figure 8b.

4.2.3 Positron annihilation lifetime spectroscopy (PALS)

In order to characterise the effect of NPA prior to AA, a so-called secondary ageing experiment was carried out. In this type of experiment, samples are artificially aged for a very short time (here 1 min) in an oil bath at 180°C. After removal from the oil bath, cooling and

drying, a PALS measurement is carried out for typically 1000 – 5000 min ($\approx$1 – 4 days) at 18°C. It is known from the literature that natural secondary ageing (NSA) even after some artificial ageing can take place in 6000 alloys and influence the positron lifetime.[22]

One experiment of this type was carried out for each of the alloys H (Figure 10a) and F (Figure 10b), the positron lifetime is given as a function of NSA time. The lifetime measured after quenching but before AA is given for each curve. Evidently, 1 min of ageing at 180°C has a huge impact on lifetime which is reduced by 0.038(0.013) ns for alloy H(F). The reduction is especially large for alloy H. Furthermore, during NSA after AA, the lifetime increases again and reaches a value of 0.211(0.213) after 1000(500) min. In alloy F, a slight indication for a decrease after 1000 min is observed.

In Al-Cu alloys the pronounced decrease of lifetime during AA has been explained by the formation of Cu-rich aggregates in which the vacancies are trapped.[24] Such Cu-rich environments are known to decrease positron lifetime due to the high electron density in copper. In Al-Mg-Si alloys, the occurrence of low lifetimes (0.198 ns in Figure 10, and even lower for longer AA times) is surprising since the annihilation lifetimes in bulk Si and Mg are 0.218 and 0.225 ns, respectively, and the annihilation lifetimes in vacancies in these elements are 0.266 and 0.253 ns, respectively.[28]

Two explanations seem possible: one could assume that vacancies embedded in clusters containing Si and/or Mg annihilate positrons more efficiently than anticipated from extrapolations from the pure elements. Mg and Si are both elements with a higher atomic volume, 23.25 and 20.02 Å^3/atom than Al (16 Å^3/atom) and if Mg and Si were compressed into the denser fcc lattice of Al, their electronic density could increase so much that the lower lifetimes become explicable. This could be the case when during ageing at 180°C ordered zones were formed. This seems possible since annealing already at 70°C for 20 min produces mono-layer zones 2.5 nm wide and 30 nm long which then grow into larger multilayer zones.[17] Another explanation is to assume that after AA clusters are formed in the supersaturated matrix in such a low density that the surrounding solute and vacancy-depleted bulk would contribute to positron annihilation with the typical lifetime component around 0.160 ns. This would explain why the lifetime in alloy H after AA is 0.01 ns lower than in alloy F since it contains approximately half the amount of solute and fewer positron traps would be formed. However, a two-component analysis of the spectra does not reveal the existence of a second lifetime component, which means that it either does not exist or cannot

be detected due to the too small separation of the bulk and the cluster lifetime. We found some evidence for the existence of a bulk lifetime component only in naturally aged samples for the first 60 (10) min after quenching alloys H (F). In the literature on other Al-alloys, it is usually assumed that most positrons are trapped by vacancies due to their high concentration and that the bulk lifetime component plays a minor role.[20] Therefore, this aspect is not entirely clear.

To explain secondary ageing it is argued that after short AA the residual solute supersaturation is still high enough to drive room temperature diffusion. According to this argument, the observed changes of the average positron lifetime during secondary ageing are due to solute redistribution within the matrix or from the matrix to the pre-existing clusters. Commonly, the re-increase of the lifetime during secondary ageing in Mg-containing alloys is attributed to Mg diffusing to the emerging clusters and further modifying their electron density. In Al-Cu(Mg) alloys it has been shown that the increase during secondary ageing[24] is no longer observed when there is no Mg in the alloy,[30] which convincingly underlines the crucial role of Mg. Similar effects have been observed by a number of other authors, e.g. for 6061 alloy[22] and Al-Zn-Mg alloys.[36] If we follow this argument, the decrease of lifetime during AA and also during simple natural ageing, see Figure 5, could be attributed to precipitation of predominantly Si into clusters or small zones possibly in conjunction with vacancies, while the re-increase of positron lifetime is due to diffusive processes involving Mg.

We observe a recovery of positron lifetime during secondary ageing for both the alloys H and F up to a final value of 0.211 and 0.213 ns, respectively. This value is close to the lifetime measured in samples naturally aged for a long time and the as-received materials before any heat treatment and represents an equilibrium situation. The time needed to reach the final value is roughly the same in the two alloys (about 1000 min). In alloy F, the relative changes are much smaller since the initial lifetime is higher. In alloy H the increase is very pronounced and if there had been a bulk component in the lifetime spectrum (0.160 ns) immediately after quenching, it vanishes during secondary ageing when many more Mg-related positron traps are formed.

The observed influence of NPA prior to AA on the secondary ageing behaviour reveals a big difference between alloys H and F. In alloy F, even a short pre-aging of just 5 min largely slows down the lifetime increase and reduces the final lifetime reached. 10 min of NPA are sufficient to prevent any lifetime change. In other words, within the first 10 min of

NPA, clustering processes occur that block the ability of the alloy to retain a supersaturation of Mg after AA that then drives secondary ageing. Possibly, during these 10 min of NPA nuclei are formed that bind a large part of the solute during the ensuing short (1 min) AA treatment. In alloy H the situation is totally different. One pronounced effect of NPA is to decrease the lifetime change caused by AA since the starting points of the 3 curves in Figure 10(a) move up towards longer lifetimes. The reason could be that during NPA the environment around the vacancies enriches in Si (which reduces the lifetime already) and that these clusters then act as seeds of further Si clustering during AA. As more clusters are formed than in the experiment without NPA, the bulk component that reduced lifetime would be reduced. This pre-clustering during NPA also affects secondary ageing after AA in a way that the slope of lifetime increase is reduced and the increase of lifetime takes place at later times. Moreover, the final lifetime reached is reduced. These facts are summarised in Figure 10(c,d), where the range of observed lifetimes from the beginning to the end of secondary ageing is displayed for both alloys.

The difference between alloy H and F is emphasised here since alloy H does not show a negative effect of NPA on AA, but alloy F does. The observation that the negative effect of NPA on AA is established in 10 min to 18 min, see above, suggests that this could be linked to the effect that blocks solute diffusion during NSA as expressed by the suppressed lifetime change.

5 Conclusions

We have shown by various methods that during natural ageing many of the observed changes of a specific property occur at similar times. Although the exact physical origin of the phenomena are not known with certainty, there is good reason to believe that the coincidences observed is not accidental but reflect different stages of precipitation. Figure 11 summarises the different stages, namely,

Stage 0 can be detected only indirectly. We assume that after quenching vacancies are freely diffusing in the alloy before they get bound by a solute atom and form solute/vacancy complexes. As the solute concentration is so high and the vacancies diffuse quickly at elevated temperatures, this could already happen during quenching. The strongest evidence for this stage is that the positron lifetime in both the alloys $2-3$ minutes after quenching is about 0.015 ns – 0.02 ns lower than that for free vacancies in Al (0.250 ns). In alloy H, we might be observing the tail of this initial decrease since the lifetime curve in stage 1 is slightly

concave as shown in Figure 5. In alloy F, no such tail of an initial decrease is observed and therefore it must have taken place much faster than in alloy H, i.e. before the first lifetime measurement, i.e. in the shaded area in Figure 5.

Stage 1 is only observed in alloy F and lasts until 7 – 10 min after quenching (at 'room temperature', longer at lower temperatures[12]). One manifestation of this stage is that the positron lifetime is nearly constant and starts to decrease only at the transition to stage 2. Moreover, 10 min of natural ageing lead to such a degree of clustering that during secondary ageing after 1 min of AA no more lifetime changes take place. Third, during this period, a different rate of the increase of electrical resistivity might be discernable in the in-situ measurements. Finally, the negative effect on hardness response during AA is largely established during this period. Microscopically, the formation of small Si-rich aggregates not entirely surrounding the vacancies attached to them and not closely packed seems possible. Such clustering would not have a big impact on the positron lifetime but provide nuclei for the next stage.

Stage 2: in this stage the positron lifetime during natural ageing decreases and reaches a minimum after about 60 min or 80 min for alloys F and H, respectively. After about the same time, both the hardness and resistivity increase in alloy F start levelling off. Finally, DSC shows that a first exothermic reaction is completed after about 60 min. Following the arguments given in the literature,[26] in this stage the vacancies would be increasingly trapped and immobilised in silicon-rich clusters that become denser and therefore give rise to a reduced lifetime of the positrons.

Stage 3: the positron lifetime during natural ageing starts increasing again in both the alloys. Slower resistivity increase, slower rate of hardening and the second cluster reaction detected in the thermal signal proceed after about the same time (>50-85 min). The diffusion of magnesium within the solid solution that is more sluggish than that of silicon now gains importance and leads to the formation of co-clusters of both Si and Mg.

Stage 4: the positron lifetime starts to decrease again (>800 min), approaching the equilibrium value very slowly. We have not investigated the long term development in this stage. For alloy F, hardness and resistivity show a slowing of rate at 800 – 1500 min during the change from stage 3 to 4. It remains to be confirmed whether this is really a defined

transition or rather a gradual change. One possible mechanism could be progressing ordering within the cluster associated with a migration of vacancies out of the clusters into the solid solution and to sinks where they annihilate.

One aspect of the measurements that awaits further clarification is that the positron lifetime evolution during NA is so similar for alloy H and F while the hardness and resistivity changes are show a clearly distinct behaviour.

Ageing processes in aluminium 6000 alloys have been investigated by many researchers but still some fundamental questions remain unsolved. Although many methods have been applied to these alloys, comparability is difficult since each group has used different alloys in terms of Mg-Si content, alloy purity or content in further elements and also alloy processing conditions. Further investigations in the future should include more studies of the role of Mg and an attempt to measure the Doppler broadening of the positron annihilation radiation during ageing which could provide the additional local chemical information needed.

Acknowledgements

References

[1]   A. Wilm, *Metallurgie* **1911**, *8*, 25.

[2]   A. Guinier, *Nature* **1938**, *142*, 569; A. Preston, *Nature* **1938**, 142, 570.

[3]   R. S. Archer, Z. Jeffries, *Trans AIME* **1925**, *71*, 828.

[4]   P. Brenner and H. Kostron, *Z. Metallkde.* **1939**, *31*, 89.

[5]   I. Polmear, *Light Alloys*, Butterworth-Heinemann, Amsterdam **2006** (4th ed.).

[6]   C. D. Marioara, S. J. Andersen, H. W. Zandbergen, R. Holmestad, *Met. Mater. Trans*. **2005**, *36A*, 691.

[7]   M. A. van Huis, J. H. Chen, M. H. F. Sluiter, H. W. Zandbergen, *Acta Mater*. **2007**, *55*, 2183.

[8]   S. J. Andersen, C. D. Marioara, R. Vissers, M. Torsaeter, R. Bjorge, F.J.H. Ehlers, R. Holmstad, *Mater. Sci. Forum* **2010**, *638-642*, 390.

[9]   J. H. Chen, E. Costan, M. A. van Huis, Q. Xu, H. W. Zandbergen, *Science* **2006**, *312*, 416.

[10]   J. Røyset, T. Stene, J. A. Sæter, O. Reiso, *Mat. Sci. Forum.* **2006**, *519-521*, 239.

[11]   H. Seyedrezai, D. Grebennikov, P. Mascher, H. S. Zurob, *Mater. Sci. Eng. A* **2009**, *525*, 186.

[12]   J. Banhart, C.S.T. Chang, M.D.H. Lay, A.J. Hill (in preparation).

[13]   C. S. T.Chang, I. Wieler, N. Wanderka, J. Banhart, *Ultramicroscopy* **2009***, 109***, 585.

[14]   A. Serizawa, S. Hirosawa, T. Sato, *Met. Mater. Trans*. **2008**, *39A*, 243.

[15]   H. Suzuki, M. Kanno, G. Itoh, *Aluminium* **1981**, *67*, 628.

[16]   M. Murayama, K. Hono, *Acta Mater*. **1999**, *47*, 1537.

[17]   K. Matsuda, S. Ikeno, *Mater. Sci. Forum* **2005**, *475-479*, 361.

[18]   T. J. Bastow, S. Celotto, *Acta Mater*. **2003**, *51*, 4621.

[19]   B. Klobes, T. E. M. Staab, E. Dudzik, *Phys. Stat. Sol. (RRL)* **2008**, *2*, 182.

[20]   A. Dupasquier, G. Kögel, A. Somoza, *Acta Mater.* **2004**, *52*, 4707.

[21]   B. Klobes, T. E. M. Staab, M. Haaks, K. Maier, I. Wieler, *Phys. Stat. Sol. (RRL)* **2008**, *2*, 224.

[22]   J. Buha, P. R. Munroe, R. N. Lumley, A. G. Crosky, A. J. Hill, in *Proc. 9th Int. Conf. Aluminium Alloys* (Eds: J. F. Nie, A. J. Morton and B. C. Muddle), Institute of Materials Engineering Australasia Ltd. **2004**, 1028.

[23]   W. Egger, G. Kögel, P. Sperr, H.-J. Gutladt, *Int. J. Mater. Res*. **2006**, *97*, 1633.

[24] A. Somoza A. Dupasquier, I. J. Polmear, P. Folegati, R. Ferragut, *Phys. Rev. B* **2000**, *61*, 14454.

[25] B. T. M. Willis, C. J. Carlisle, *Experimental Neutron Scattering* **2009,** Oxford University Press, Oxford.

[26] S. Esmaeli, W. J. Poole, D. J. Lloyd, *Mater. Sci. Forum* **2000**, *331-337*, 995.

[27] C. S. T. Chang, Z. Liang, J. Banhart, Scripta Mater. **2010** (submitted).

[28] A. Seeger, F. Banhart, *Phys. Stat. Sol (a)*, **1987**, *102*, 171.

[29] H. S. Zurob, H. Seyedrezai, *Scripta Mater.* **2009**, *61*, 141.

[30] R. Ferragut, G. Ferro, M. Biasini, in *Proc. 9th Int. Conf. Aluminium Alloys* (Eds: J. F. Nie, A. J. Morton and B. C. Muddle), Institute of Materials Engineering Australasia Ltd. **2004**, 1022.

[31] P. Donnadieu, F. Carsughi, A. Redjaima, C. Diot, G. Lapasset, *J. Appl. Cryst.* **1998**, *31*, 212.

[32] R. Schiffmann, J. Haug, J. Banhart, in *Proc. 9th Int. Conf. Aluminium Alloys* (Eds: J. F. Nie, A. J. Morton and B. C. Muddle), Institute of Materials Engineering Australasia Ltd. **2004**, 604.

[33] A. K. Gupta, D. J. Lloyd, *Met. Mater. Trans. A* **1999**, *30A*, 879.

[34] C. S. Tsao, C.-Y. Chen, U.-S. Jeng and T.-Y. Kuo, *Acta Mater.* **2006**, *54*, 4621.

[35] P. L. Rossiter, *The electrical resistivity of metals and alloys*, Cambridge University Press, Cambridge **1987**.

[36] A. Dupasquier, R. Ferragut, M. M. Iglesias, M. Massazza, G. Riontino, P. Mengucci, G. Barrucca, C. E. Macchi, A. Somoza, *Phil. Mag.* **2007**, *87*, 3297.

[37] H. Rauch, W. Waschkowski, in *Neutron data booklet* (Eds. A.-J. Dianoux, G. Lander) ocp science, Philadelphia **2003.**

[38] L. A. Feigin, D. I. Svergun, *Structure analysis by small-angle X-ray and neutron scattering*, Plenum Press, New York **1989.**

[39] F. R. Fickett, *Cryogenics* **1971**, *11*, 349.

[40] R. Vissers, M. A. van Huis, J. Jansen, H. W. Zandbergen, C. D. Marioara, S. J. Andersen, *Acta Mater.* **2007**, *55*, 3815.

[41] J. A. Nock, *The Iron Age* **1947**, *159*, 48.

[42] P. E. Fortin, *Can. Met. Qtly.* **1963**, *2*, 143.

[43] D. W. Pashley, J. W. Rhodes, A. Sendorek, *J. Inst. Metals* **1966**, *94*, 41.

[44] R. C. Dorward, *Met. Trans*. **1973**, *4*, 507.

[45] H. Kimura, R. R. Hasiguti, *Trans. JIM* **1975**, *16*, 361.

[46] A. Serizawa, S. Hirosawa, T. Sato, *Mater. Sci. Forum* **2006**, *519-521*, 245.

[47] I. Dutta, S. M. Allen, *J. Mater. Sci. Lett.* **1991**, *10*, 323.

[48] R. M. Nieminen, J. Laakkonen, *Appl. Phys.* **1979**, *20*, 181.

[49] A. Ried, P. Schwellinger, H. Bichsel, *Aluminium* **1977**, *53*, 595.

[50] C. Panseri, T. Federighi, *J. Inst. Metals* **1966**, *94*, 99.

[51] H. S. Hasting, A. G. Froseth, S. J. Andersen, R. Vissers, J. C. Walmsley, C.D. Marioara, F. Danoix, W. Lefebvre, R. Holmstad, *J. Appl. Phys* **2009**, *106*, 123527.

[52] S. Ceresara, E. Di Russo, P. Fiorino, A. Giarda, *Mater. Sci. Eng.* **1969**, *5*, 220.

[53] Z. Liang, Thesis, South China University of Technology, **2009**.

[54] C. D. Marioara, S. J. Andersen, J. Jansen, H. W. Zandbergen, *Acta Mater.* **2003**, *51*, 789.

[55] M. A. Van Huis, M. H. F. Sluiter, J. H. Chen, H. W. Zandbergen, *Phys. Rev. B* **2007**, *76*, 174113.

[56] C. N. Aiza Jaafar, G.W. Lorimer, N.C. Parson. *Mater. Sci. Forum* **2006**, *519-521*, 227

[57] A. Latkowski, M. Bronicki, *Aluminium* **1989**, *65*, 391.

[58] K. Matsuda, H. Gamada, K. Fujii, Y. Uetani, T. Sato, A. Kamio, S. Ikeno, Met. Mater. Trans. **1998**, *29A*, 1161.

[59] G. A. Edwards, K. Stiller, G. L. Dunlop, M. J. Couper, *Acta Mater.* **1998**, *46*, 3893.

[60] A. Serizawa, T. Sato, in *Aluminium Alloys* (Eds. J. Hirsch, B. Skrotzki, G. Gottstein) Wiley-VCH, Weinheim **2008**.

[61] I. Kovács, J. Lendvai, E. Nagy, *Acta. Met.* **1972**, *20*, 975

[62] Y. Yamada, T. Sato, A. Kamio, *Mater. Sci. Forum* **2000**, *331-337*, 669

[63] M. Takeda, F. Ohkubo, T. Shirai, F. Fukui, *J. Mater. Sci.* **1998**, *33*, 2385

[64] A. Kelly, R. B. Nicholson, *Prog. Mater. Sci.* **1963**, *10*, 151, especially p. 176

6 Figure captions
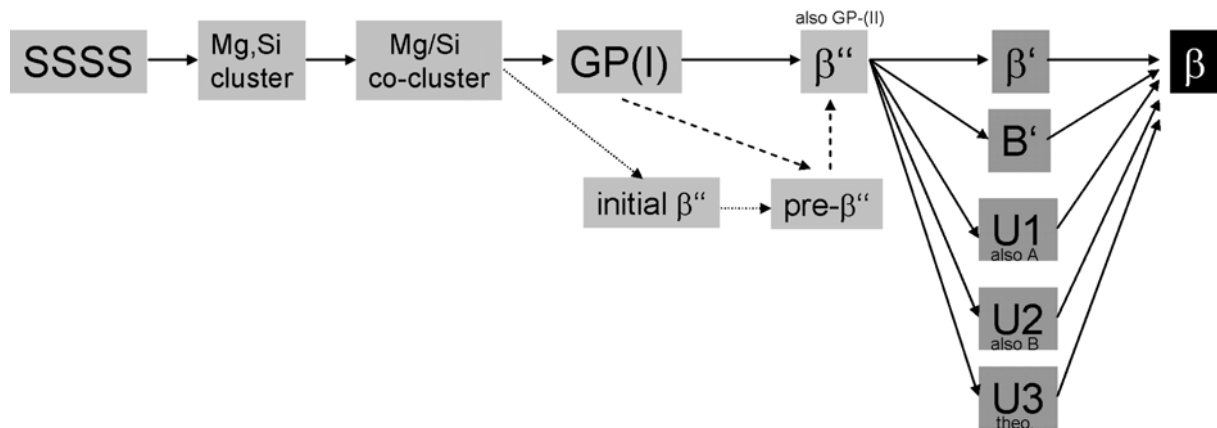
Figure 1. Sequence of phases found during age hardening of Al-Mg-Si alloys. Compiled from various sources in the literature[5,7,40]. Supersaturated solid solution (SSSS) decomposes as Mg and Si atoms are attracted first to themselves (cluster) then to each other (co-cluster) to form precipitates GP(I), sometimes also called initial-β''. GP(I) zones either further evolve directly to a phase β'' and then to a number of other metastable phases labelled β', B', U1, U2 (another one, U3, has been postulated theoretically), or first form an intermediate phase called pre-β''. The sequence depends on the Mg and Si content and the temperatures applied. The final equilibrium phase β is reached for higher temperatures only.[5]
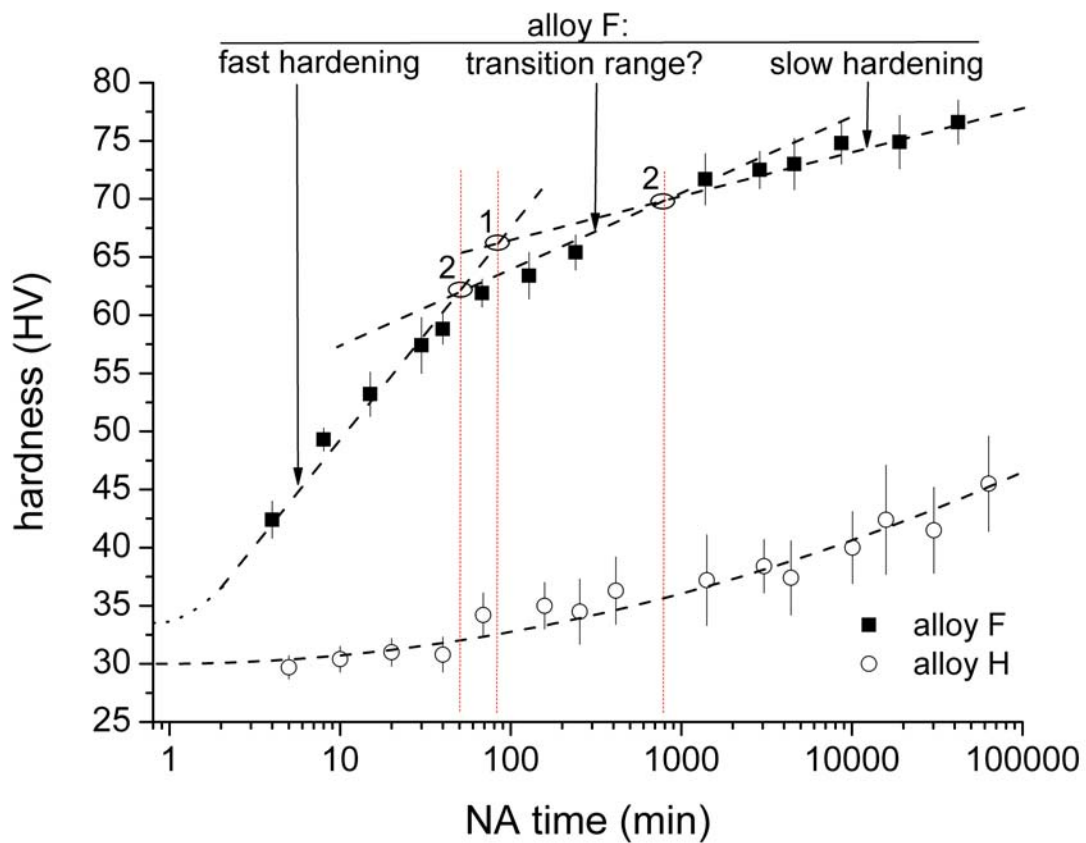
Figure 2. Hardness evolution of alloys H and F during NA at 20°C after solutionising and quenching. Each point represents the average of 10 individual hardness measurements and the corresponding statistical error. The vertical dotted lines separate ranges in which the logarithmic increase for alloy F follows straight lines of distinct slopes. The labels '1' and '2' denote the times of crossover between different slopes, assuming either two or three different regimes. Broken lines are best fits.
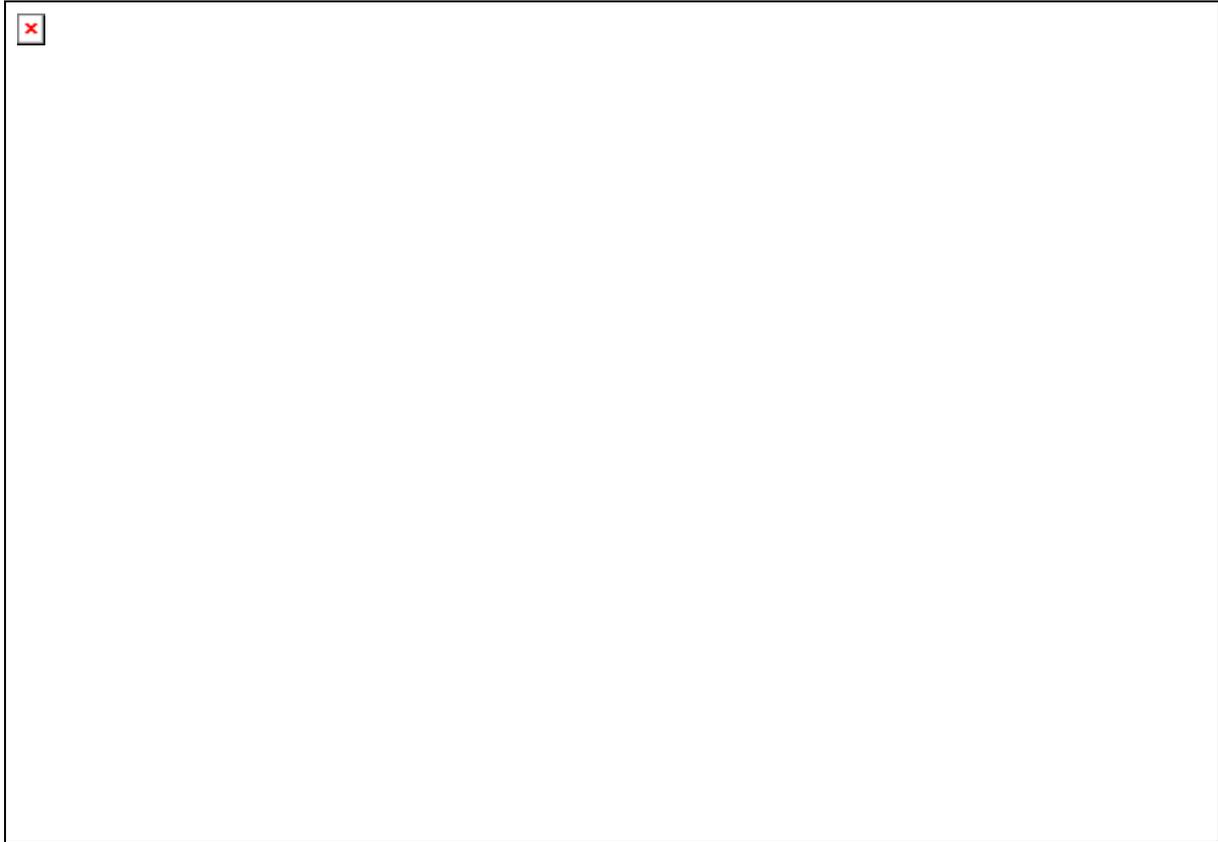
Figure 3. Evolution of electrical resistivity of alloy F during natural ageing at 21°C after solutionising and quenching. The time resolution of the measurement is 0.3 s. The broken lines indicate ranges where the resistivity increases as log(t), which is disputable for the initial stage. The dash-dotted line is a linear fit to the resistivity data up to 10 min (appearing as an exponential in this representation). Data for alloy H measured with a lower time resolution is displayed for matters of comparison (right axis).
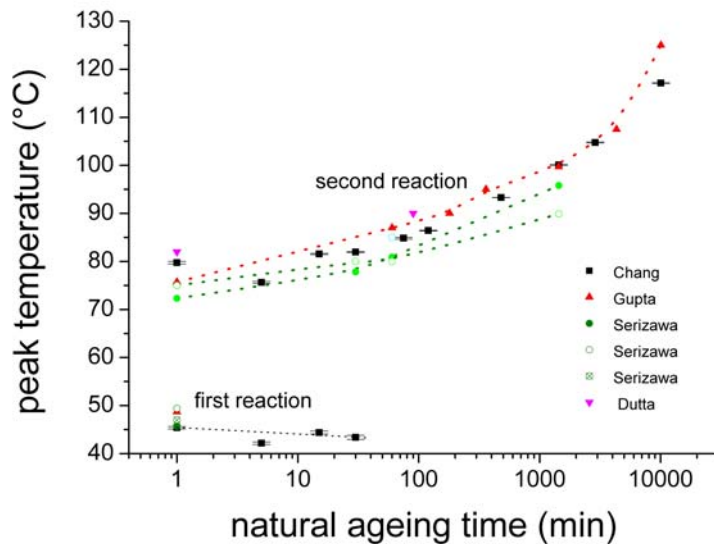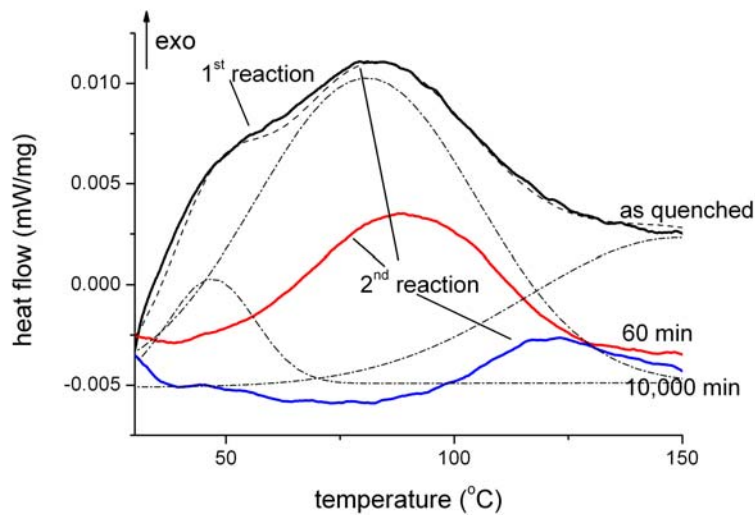
Figure 4. a) DSC traces at 10 K/minfor alloy F after solutionising, quenching and optional NA: i) DSC directly after quenching ('as-quenched', technically 1 min NA), ii) 60 min of NA, iii) 10,000 of NA. Temperature range restricted to 25 – 150°C to emphasise the cluster formation peaks. The broken lines are decompositions of the 'as-quenched' curve into 3 Gaussians. b) DSC peak position as measured by different authors as a function of NA time: Chang[27], Gupta[33], Serizawa[46,46,14], Dutta[47].
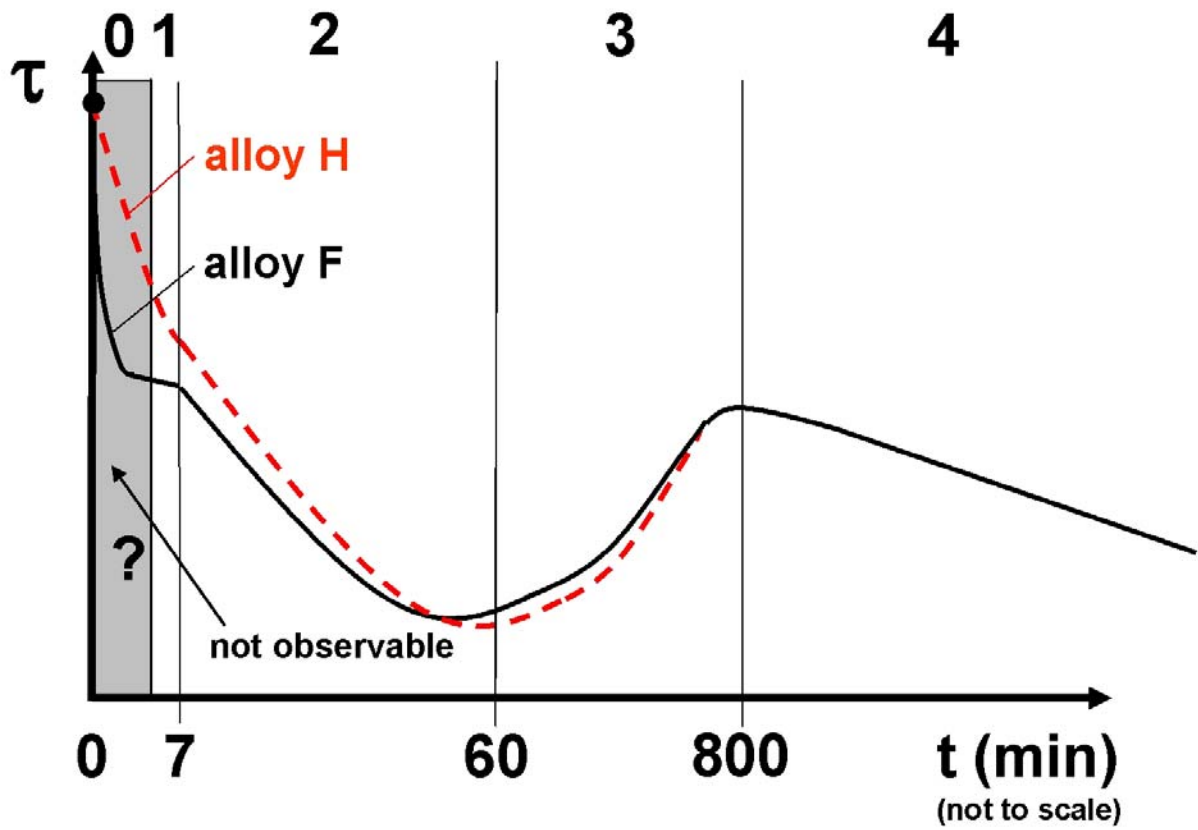
Figure 5. Schematic course of the average positron lifetime measured in Al-Mg-Si alloys during natural ageing directly after solutionising and quenching.[12] approximate NA times are given. Black dot corresponds to positron lifetime of free vacancies in Al (0.250 ns) which is considered the starting point of the curve.
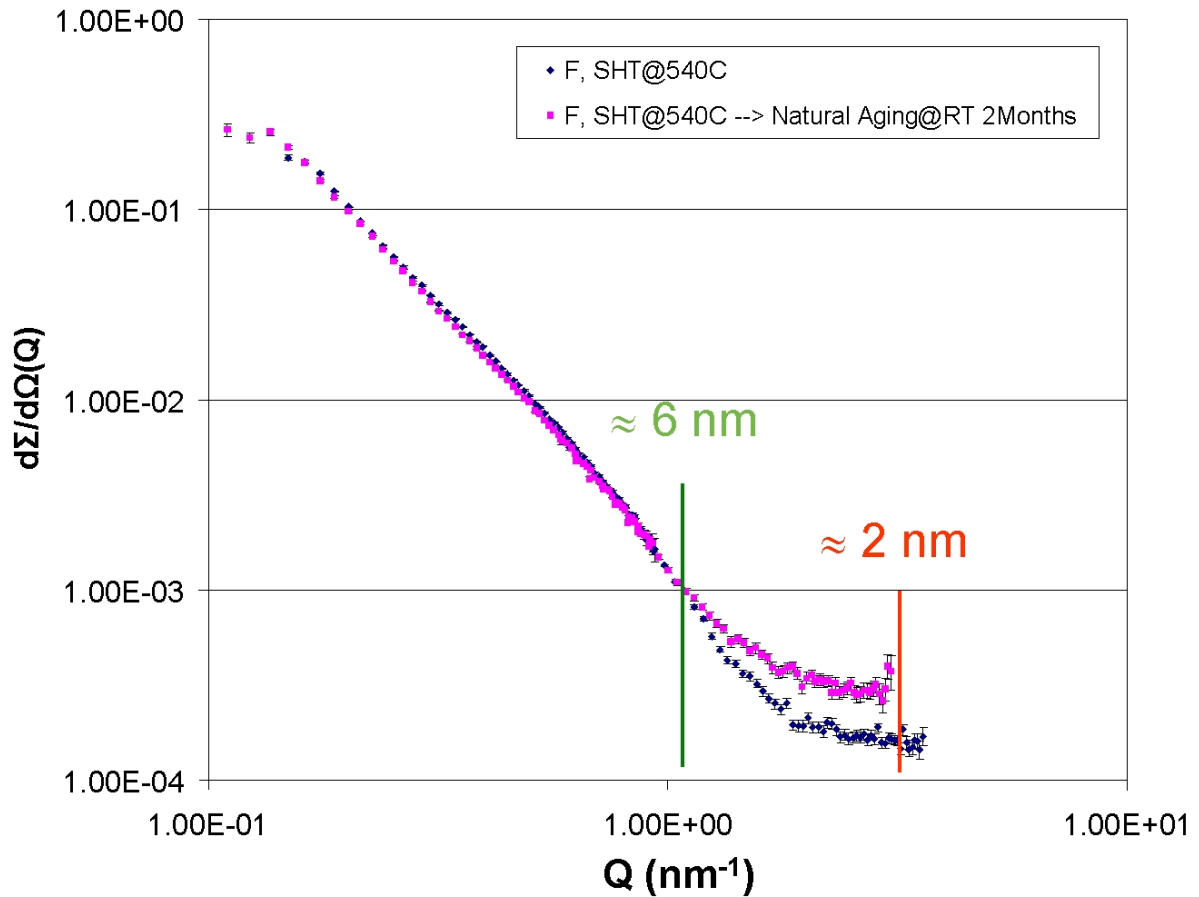
Figure 6. Small-angle neutron scattering curve of an alloy F sample measured either directly after solutionising and quenching or after another 87,000 min (2 months) of natural ageing. The actual SANS measurement took 240 min and was carried out at 'room temperature'. Vertical bars mark the typical size ranges $R = 2\pi/Q$ a particular scattering vector Q stands for.

volume: 7 nm x 7 nm x 164 nm

● Mg ● Si
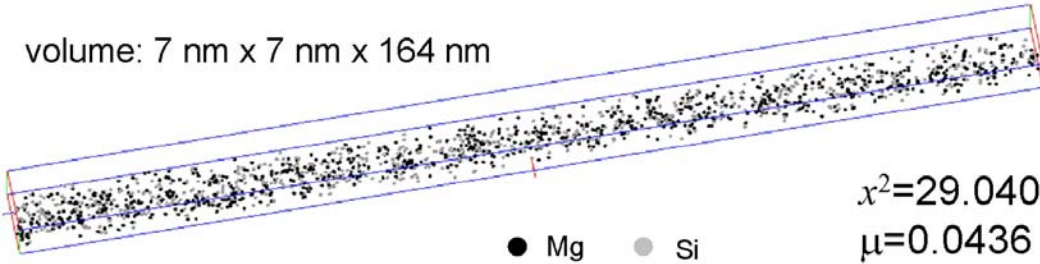
$x^2 = 29.0409$
$\mu = 0.0436$

contingency table analysis:

measured results

		Si		
		0	1	≥ 2
Mg	0	8957	2675	661
	1	1731	603	185
	≥ 2	293	109	33
				15247

expected (random)

		Si		
		0	1	≥ 2
Mg	0	8854	2731	709
	1	1814	560	145
	≥ 2	313	97	25
				15247

trend analysis

		Si		
		0	1	≥ 2
Mg	0	+	-	-
	1	-	+	+
	≥ 2	-	+	+

+ ~ number $_{measured}$ > number $_{expected}$
- ~ number $_{measured}$ < number $_{expected}$
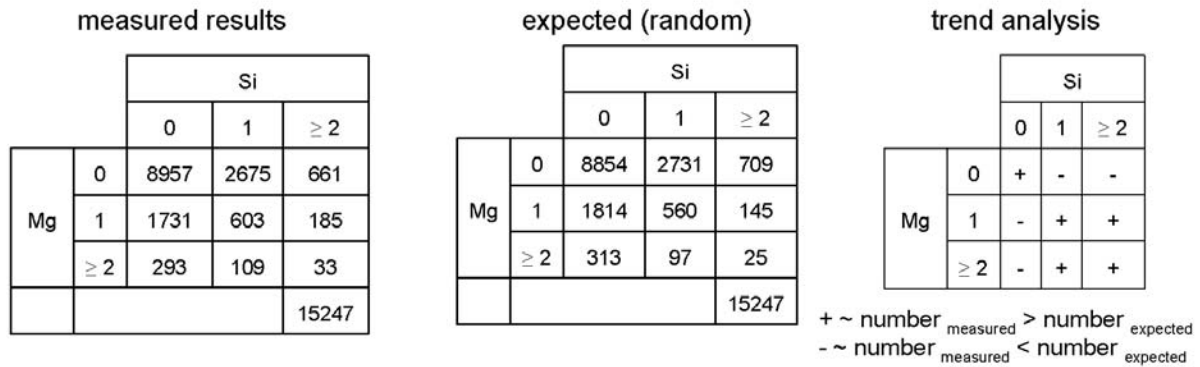
Figure 7. Atom probe analysis of alloy F naturally aged for 260,000 min (6 months) after solutionising and quenching. Top part: 3D rendering of Mg and Si atom positions in the volume specified. Aluminium atoms have been omitted. Lower part: corresponding contingency tables. They can be read as follows: The number on the upper left of the table gives the number of blocks that neither contain Mg nor Si ('0-0'). The second number in the first column gives the number of blocks that contain no Si but one Mg atom ('1-0'), and so on. The table labelled 'expected' gives values representing a random distribution of Mg and Si in the entire volume. A comparison of the observed and expected values is given in the table labelled 'trend analysis'.
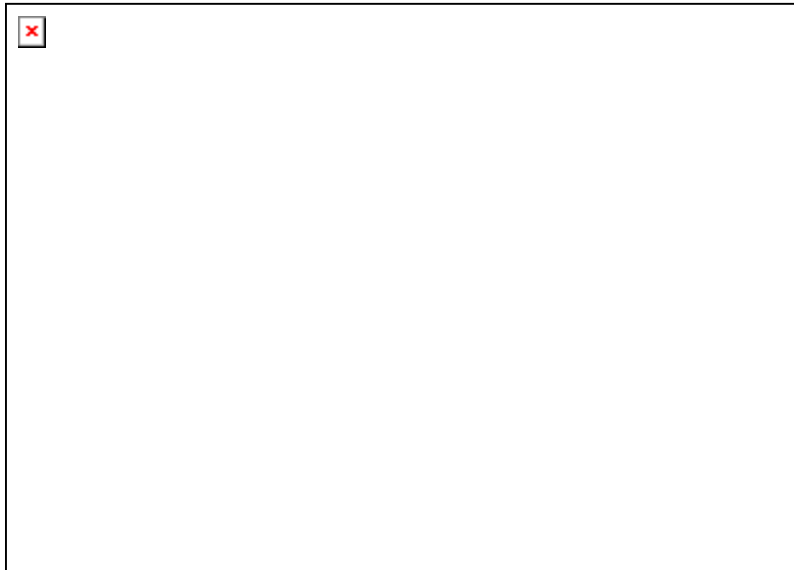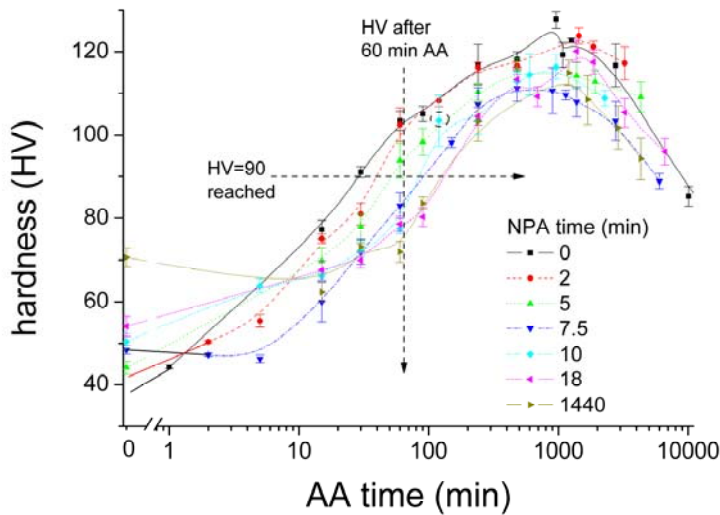
Figure 8. (a) Evolution of hardness in alloy F during artificial ageing at 180°C that is carried out after solutioning, quenching and different ensuing natural pre-ageing (NPA) treatments ranging from '0' to 1440 min.

(b) Display of different quantities after a given NPA time: hardness reached after 60 min of AA, time to reach a hardness level of 90HV (omitting the point encircled in Figure 8a), change in positron lifetime during secondary ageing (difference values calculated from data in Figure 10). Note that the value for 'no NPA' is set to 0.1 min to allow for display on the logarithmic scale which is a realistic but not an exactly measured delay time. A critical change occurs from >2 min to 18 min of NPA at 'room temperature' and this critical change is defined as the *negative effect*.
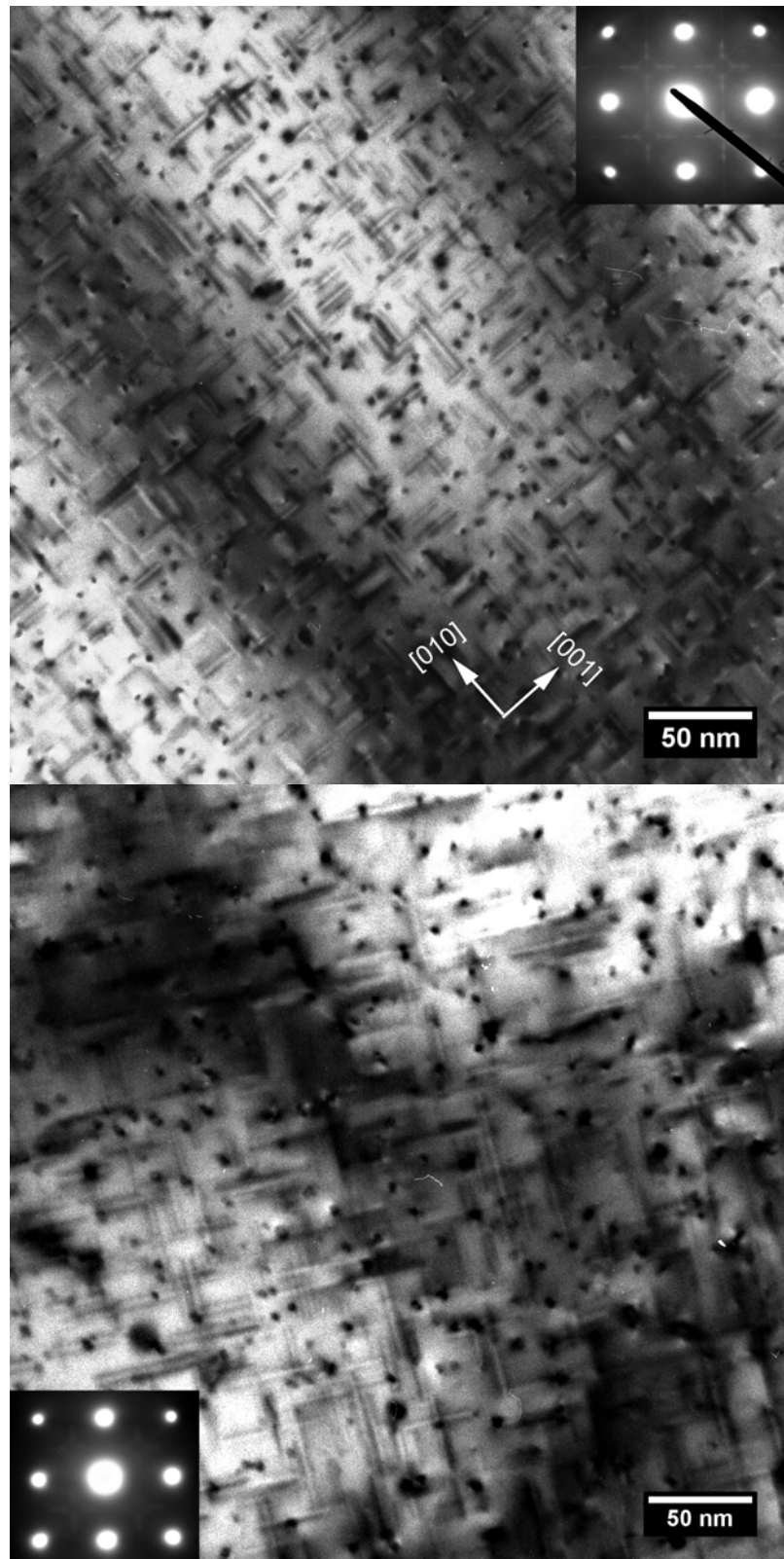
Figure 9. Transmission electron microscopy images of alloy F subjected to 2 different heat treatments. (a) solutionising and quenching, immediate AA at 180°C for 540 min, (b) solutionising and quenching, natural ageing for 10,000 min at 20°C, AA at 180°C for 540 min[53]. Hardness values corresponding to these images are 118 and 110 HV.

τ (ns) after NPA but before AA

0.218

0.215

0.229

0.236

(a)

0.217   0.223   0.222

0.214   0.219

natural pre-ageing (NPA)
——— 0 min
– – – 5 min
········· 10 min
–·–·– 40 min
–··–··– 1440 min

(b)

°C

535   SHT

180   AA

18   NPA   NSA

0   t

NSA time (min)

34
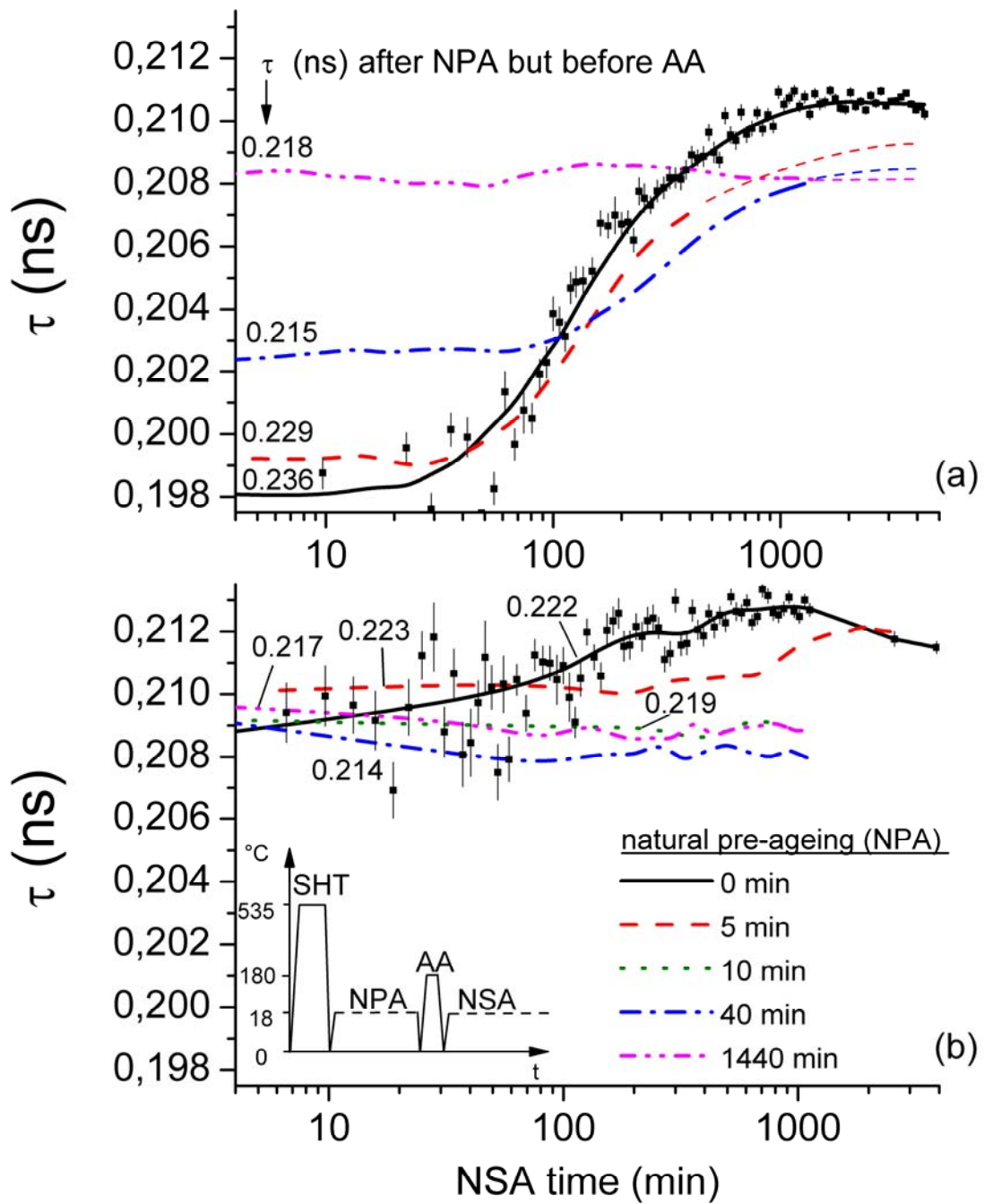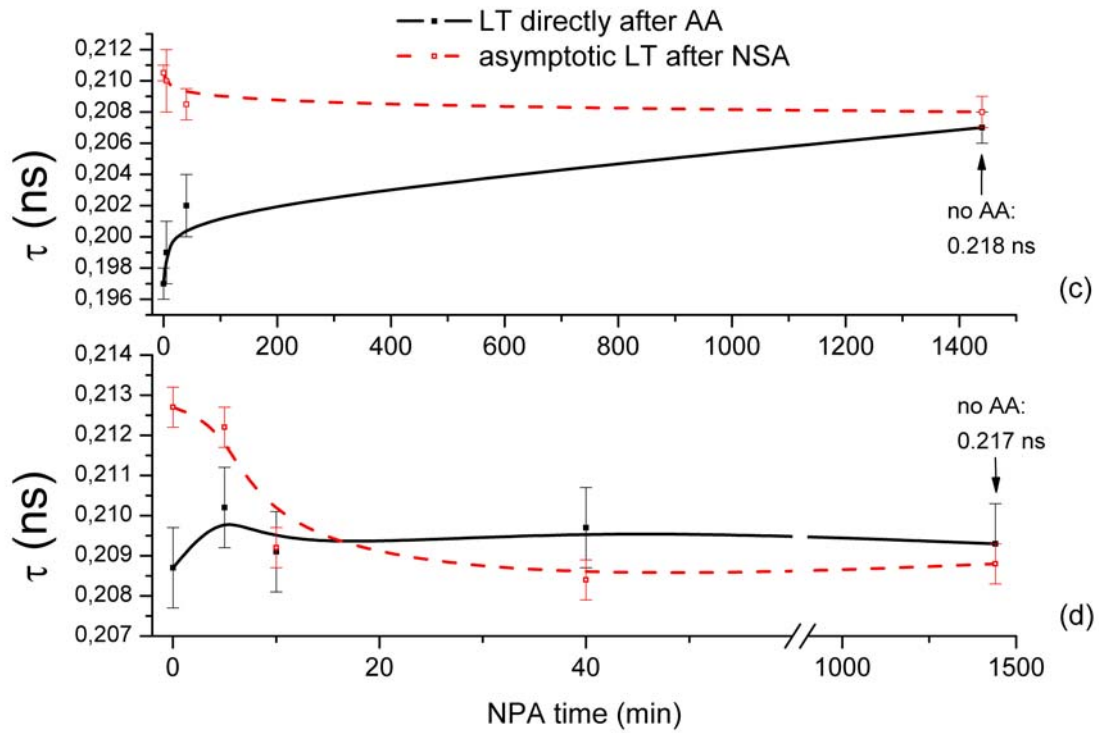
Figure 10. Positron lifetimes in alloys H (a,c) and F (b,d).

a,b) lifetime evolution during secondary ageing at 18°C after natural pre-ageing at 18°C and artificial ageing for 1 min at 180°C (see schematic temperature course in Figure 10b). Individual data points are shown just for one of the curves, otherwise interpolated and smoothed data are given to keep the graphs simple. Broken lines are extrapolations where there is a gap in the available data. The lifetimes immediately before AA are given for each curve.

c,d) lifetime before and estimated asymptotic lifetime after secondary ageing as a function of NPA time. Note that different time scales are used for the alloys.
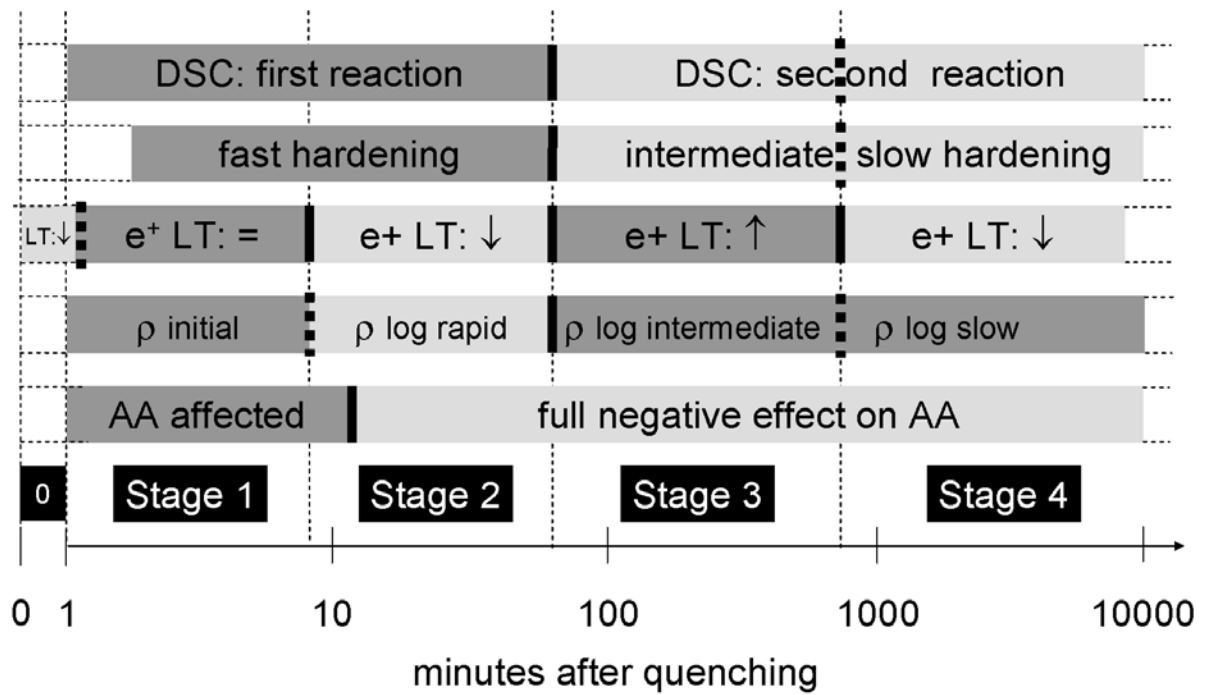
Figure 11. Schematic comparison of different characteristic lifetimes identified in the current study: e^+ LT = positron lifetime and the direction of change is indicated, ρ is electrical resistivity, 'AA affected' is range where negative effect of NPA on AA develops, in the range after the negative effect is fully established. Short vertical bars indicate transitions between stages that can be clearly identified experimentally, dotted bars indicate transitions that appear less clear or are theoretical. Horizontal dotted lines mark time domains in which no experimental data is available.

7 Tables

Table 1. Coherent and incoherent scattering length for thermal neutrons (λ=0.18 nm),[37] coherent X-ray cross section calculated from the Thomson formula b_{coh} =Z×2.82 fm[38] and position of X-ray absorption edge for the three elements Mg, Al, Si.

element	b_{coh} (fm)	b_{incoh} (fm)	$b_{coh}(q{\approx}0)$[a] (fm)	K-edge (keV)
	thermal neutrons			X-rays
Mg	5.38	0	33.84	1.31
Al	3.45	0.26	36.66	1.56
Si	4.15	0	39.48	1.84

[a] far away from absorption edges, near-forward scattering

Table 2. Alloy compositions as determined by OES (Optical Emission Spectroscopy)

alloy code	Mg[a]	Si[a]	Fe[b]	Mn[b]	Cu[b]	Cr[b]	Bi[b]	Sn[b]	others[b,c]
H	0.40	0.40	<5	<2	<2	<2	<10	<10	<5
F	0.59	0.82	<5	<2	<2	<2	<10	<10	<5

[a] in % by mass
[b] in ppm by mass
[c] Ni, Zn, Ti, B, Be, Ca, Cd, Co, Ga, In, Li, Na, P, Pb, Sb were analysed

Table 3. Precipitate length and density as derived from TEM images of alloy F solutionised, quenched, naturally pre-aged at ‚room temperature' for the time specified and finally aged for 540 min at 180°C.[53]

NPA time (min)	0	5	18	10,000
length (nm)	15±4	16±3	24±7	27±7
diameter (nm)	3.6±0.7	3.6±0.7	4.3±0.9	4.8±0.9
density (10^{22} m^{-3})	12.7±1.3	11.5±0.5	8.7±0.9	8.3±0.5
volume fraction (%)	2.5	2.3	4.0	5.1